HHS Public Access

Author manuscript

Matrix Biol. Author manuscript; available in PMC 2022 August 01.

Published in final edited form as:

Matrix Biol. 2021 August ; 102: 70–84. doi:10.1016/j.matbio.2021.07.001.

PAD2-mediated citrullination of Fibulin-5 promotes elastogenesis

Bo Sun[1,2], **Beverly Tomita**[1,2], **Ari Salinger**[3], **Ronak R. Tilvawala**[3], **Ling Li**[4], **Hana Hakami**[4], **Tao Liu**[2,5], **Konstantin Tsoyi**[6], **Ivan O. Rosas**[6], **Dieter P. Reinhardt**[4], **Paul R. Thompson**[3], **I-Cheng Ho**[1,2,*]

[1]Division of Rheumatology, Inflammation, and Immunity, Department of Medicine, Brigham and Women's Hospital, Boston, MA 02115

[2]Harvard Medical School, Boston, MA 02115

[3]Department of Biochemistry and Molecular Pharmacology, University of Massachusetts Medical School, Worcester, MA 01605

[4]Department of Anatomy and Cell Biology and Faculty of Dentistry, McGill University, Montreal, QC H3A 0C7, Canada

[5]Division of Allergy and Clinical Immunology, Department of Medicine, Brigham and Women's Hospital, Boston, MA 02115

[6]Pulmonary, Critical Care and Sleep Medicine Section, Baylor College of Medicine, Houston, TX 77030

Abstract

The formation of elastic fibers is active only in the perinatal period. How elastogenesis is developmentally regulated is not fully understood. Citrullination is a unique form of post-translational modification catalyzed by peptidylarginine deiminases (PADs), including PAD1-4. Its physiological role is largely unknown. By using an unbiased proteomic approach of lung tissues, we discovered that FBLN5 and LTBP4, two key elastogenic proteins, were temporally modified in mouse and human lungs. We further demonstrated that PAD2 citrullinated FBLN5 preferentially in young lungs compared to adult lungs. Genetic ablation of PAD2 resulted in attenuated elastogenesis *in vitro* and age-dependent emphysema *in vivo.* Mechanistically, citrullination protected FBLN5 from proteolysis and subsequent inactivation of its elastogenic activity. Furthermore, citrullinated but not native FBLN5 partially rescued *in vitro* elastogenesis in the absence of PAD activity. Our data uncover a novel function of citrullination, namely promoting elastogenesis, and provide additional insights to how elastogenesis is regulated.

*Correspondence to: I-Cheng Ho; 60 Fenwood Road, Boston, MA 02115; Tel: 617-5251005; Fax: 617-5251010; iho@bwh.harvard.edu.

The authors declared that no conflict of interest exists.

Keywords

citrullination; deimination; deiminase; elastic fiber; Fibulin-5; lung compliance

Introduction

The assembly of tropoelastin (TE) into elastic fibers requires a complex hierarchical action of several proteins including but not limited to the following key events [1, 2]. TE, once secreted by elastogenic cells, such as fibroblasts or vascular smooth muscle cells undergoes self-association on the cell surface. This step is facilitated by short fibulins, including Fibulin-4 (FBLN4) and Fibulin-5 (FBLN5). These TE microassemblies along with FBLN4/5 are then deposited onto microfibrils, which consist of mainly Fibrillin-1 (FBN1) and Fibrillin-2 (FBN2). The recruitment of TE microassemblies to microfibrils requires Latent Transforming Growth Factor Beta Binding Protein-4 (LTBP4). The final step of elastogenesis is extensive cross-linking of TE along microfibrils by Lysyl Oxidase (LOX) and Lysyl Oxidase Like-1 (LOXL1), which are recruited by FBLN4/5 and activated by proteolytic cleavage. Loss of function mutations in any of the genes involved in the assembly/cross-linking of TE results in cutis laxa [3], featuring loose skin, congenital emphysema, and tortuosity of aorta.

Elastic fibers, with a half-life estimated at approximately 80 years in human [4], are highly durable. It is not surprising that elastogenesis is a developmentally regulated process, starting at mid-gestational age and ending in the postnatal period. One known mechanism regulating the temporal pattern of elastogenesis is down-regulation of TE expression [5]; however, additional mechanisms very likely exist. For example, reexpression of TE has been reported in end stage chronic obstructive lung disease (COPD) [6, 7], but no regeneration of functional elastic fibers *in vivo* has been observed. Reversely, excessive formation of elastic fibers is a pathological feature of pleuroparenchymal fibroelastosis, a unique form of interstitial lung disease without an effective treatment [8]. Thus, elucidating the additional mechanisms regulating elastogenesis will eventually lead to novel approaches of regenerating functional elastic fibers or inhibiting pathological elastogenesis.

Citrullination, also known as deimination, is a unique form of post-translational modification of proteins, in which positively charged peptidylarginine is converted to neutral non-coding peptidylcitrulline [9]. This process is catalyzed by peptidylarginine deiminases (PADs) 1-4 in mammals in a calcium dependent manner. Placental mammals carry an additional PAD, namely PAD6, which is enzymatically inactive. Citrullination can potentially affect the folding and function of proteins. Genetic or pharmacological inhibition of PAD1 leads to an arrest of embryogenesis at the 4-cell stage [10]. Genetic deficiency of PAD2 or PAD4 does not lead to any gross developmental defect; however, PAD2 and PAD4 have been shown to citrullinate histones and transcription factors [11-16], thereby altering gene expression in immune and non-immune cells. In addition, PAD4-mediated citrullination of histones facilitates decondensation of chromatin and is essential for the formation of neutrophil extracellular traps [17, 18]. In addition to intracellular proteins, proteins that are critical for the formation/function of extracellular matrix are also regulated by

citrullination. For example, null mutations in PADI3 cause "uncombable hair syndrome" and central centrifugal cicatricial alopecia in humans due to impaired cross-linking between trichohyaline and keratin [19, 20]; citrullinated Matrix Metallopeptidase 9 (MMP9) acquires a higher affinity for gelatin is more efficiently activated by MMP3 [21]; and citrullination of fibronectin alters integrin clustering and supports a more migratory/invasive phenotype of fibroblasts [22].

To characterize the role of citrullination in development, we adopted an unbiased comparative chemoproteomic approach to identify lung proteins that are developmentally citrullinated and discovered that FBLN5 and LTBP4 were preferentially citrullinated in young lungs compared to adult lungs. We showed that pharmacological inhibition or genetic ablation of PAD2 facilitated the cleavage of FBLN5 and attenuated elastogenesis. Furthermore, citrullinated FBLN5 but not native FBLN5 partially restored elastogenesis in the absence of PAD activity. More importantly, mice deficient in PAD2 spontaneously developed late onset of emphysema. Our data uncover a new mechanism regulating elastogenesis and may lead to novel approaches toward treating diseases caused by destruction of elastic fibers or pathological elastogenesis.

Results

Temporal changes in post-translational modification in lung

PAD1 and PAD3 play critical roles in embryogenesis and/or development. We therefore postulated that the citrullinome changes during development. As a model organ, we chose lung and used F95 antibody, a mouse monoclonal IgM raised against a deca-citrullinated peptide [23], to examine the level of citrullinated proteins. We found a temporal increase in the level of F95-reactive proteins (Supplemental Figure 1A). Similar results were obtained when we examined other organs, such as spleen, colon, kidney, liver, and heart. This temporal increase in the level of F95-reactive proteins was also observed in human lungs regardless of the biological sex (Supplemental Figure 1B), and was also detected with AMC (Supplemental Figure 1B), another antibody for citrullinated proteins [24]. F95 and AMC did not provide the information on the identity of the citrullinated proteins; the increased detection could be due to higher affinity to the antibodies (a qualitative change) and/or more abundant antibody-reactive proteins (a quantitative change). Interestingly, there was no temporal change in the level of citrullinated histone H3 (cit-H3) in both mouse and human lungs. We subsequently analyzed the mouse lung extract with Rhodamine-phenylglyoxal (PG) that chemically reacts with peptidylcitrulline. The overall level of PG-labeled proteins was comparable between young and adult lungs (Supplemental Figure 1C). Despite the comparable levels, some proteins were more prominent in adult lungs (arrow), whereas some were more prominent in young lungs (arrow head). Taken together, these results suggest that the lung citrullinome undergoes temporal changes; the changes are very likely bi-directional and do not occur in every protein.

Temporal changes in PG-tagged lung proteome

To identify the proteins that are temporally citrullinated in lung, we used biotinylated-PG to covalently modified citrullinated proteins from lung extracts of young (3-week-old, N=3)

and adult (6-month-old, N=4) C57BL/6 mice. The PG-tagged proteins were captured with streptavidin-conjugated beads and then subjected to mass spectrometry (Figure 1A). Spectral counts were performed to quantify changes in protein citrullination as a function of age. From this analysis, we identified 884 proteins (Supplemental Table 1). Many of the proteins had low spectral counts (less than 10) across samples and were therefore excluded. We subsequently carried out two separate comparisons of the remaining proteins. To identify PG-tagged proteins that were enriched in young lungs, we included proteins that had a spectral count ≥ 10 in all three young samples. Similarly, we included proteins that had a spectral count ≥ 10 in all four adult samples for identification of PG-tagged proteins that were enriched in adult lungs. A fold change of ≥ 1.5, $p < 0.02$, and FDR <0.1 were used to select candidate proteins. We found 35 PG-tagged proteins that were enriched in young lungs and only 4 PG-tagged proteins that were enriched in adult lungs (Figure 1B, 1C and Supplemental Table 2 & 3).

Next, we used the Human Protein Reference Database (http://www.hprd.org) and Euk-mPLoc 2.0 [25] to determine the primary subcellular localization of the differentially enriched PG-tagged proteins. Approximately 50% of the proteins are cytoplasmic proteins and the rest can be found in several other locations, including extracellular space, endoplasmic reticulum (ER) and nucleus (Figure 1D), indicating that the PG-tagged proteins are not limited to a specific subcellular localization. We subsequently used STRING [26] to identify the biological processes that are represented by the 35 PG-tagged proteins enriched in young lungs. The top two biological processes are *actin cytoskeletal organization* and *small molecular synthetic* pathways (Figure 1E). In addition, two of the top three PG-tagged proteins that were enriched in young lungs, namely FBLN5 and LTBP4, are essential for elastogenesis [27-30], whereas three of the four PG-tagged proteins that were enriched in adult lungs, namely SERPINA3K, MUG1, and A2M, are protease inhibitors, whose activity has been shown to be regulated by citrullination [31].

Confirmation of the temporal changes in PG-tagged lung proteome

The enrichment of PG-tagged proteins in one age group can be due to differences in the total amount of proteins but not necessarily in the degree of citrullination. For example, SERPINA3K, MUG2, and A2M are expressed almost exclusively in liver and their expression increases along with age in mice according to PubMed Gene. To confirm the mass spec data, we again used streptavidin to pull down PG-tagged proteins from young and adult mouse lungs. The crude lung extract (input) and PG-tagged proteins were examined with western blotting using anti-FBLN5. We indeed found a high level of PG-tagged FBLN5 in young lungs (Figure 1F). By contrast, almost no PG-tagged FBLN5 was detected in adult lungs despite a comparable level of total FBLN5. A similar temporal decrease in the level of PG-tagged FBLN5 was also observed in human lungs between 20-29 years of age and 56-65 years of age (Figure 1G). Reversely, the levels of PG-tagged and total Cytochrome P450 2F2 (Cyp2f2) were higher in adult lungs compared to young lungs, but the ratio between PG-tagged and total Cyp2f2 was still higher in adult lungs (Figure 1H). Thus the enrichment of PG-tagged Cyp2f2 in adult lungs is probably due to both an increase in the total level and the degree of citrullination.

Temporal citrullination of FBLN5 by PAD2

F95, AMC and PG recognize both citrullinated and homo-citrullinated proteins. Thus, the temporal changes in the level of PG-tagged proteins could be due to temporal citrullination and/or homo-citrullination. Homo-citrullination is a non-enzymatic process, whereas citrullination is catalyzed by PADs. The transcript level of PAD2 was the highest among PADs in lungs and the level of each PAD was comparable between young and adult lungs (Figure 2A). We therefore used lungs of WT DBA/1J and PAD2-deficient (PAD2KO) mice, which are also on DBA/1J genetic background, to determine whether the temporal change in the level of PG-tagged proteins was due to temporal citrullination. The temporal difference in the level of PG-tagged FBLN5 was still observed in WT mice but was almost abolished in PAD2KO mice (Figure 2B). There was no apparent difference between male and female mice. These results indicate that the temporal change in the level of PG-tagged FBLN5 seen in Figure 1F is mainly due to preferential citrullination of FBLN5 by PAD2 in young lungs compared to adult lungs. In addition, this temporal FBLN5 citrullination is independent of genetic background or biological sex. The residual PG-tagged FBLN5 seen in PAD2KO lungs could be PAD4-(or other PADs) citrullinated FBLN5 or homo-citrullinated FBLN5. Reversely, the increase in the level of PG-tagged Cyp2f2 in adults lungs was completely nullified by PAD2 deficiency (Figure 2C), suggesting that Cyp2f2 is also a PAD2 substrate and that PAD2 citrullinates Cyp2f2 preferentially in adult lungs compared to young lungs. This temporal pattern is in sharp contrast to that of FBLN5 and suggests that the activity of PAD2 is temporally regulated in a protein specific fashion in lung.

To further confirm that FBLN5 is a PAD2 substrate, we recombinantly produced human FBLN5 carrying a His-tag at its C-terminus (FBLN5-His) in HEK293 cells and purified it after secretion into the culture medium as described previously (Figure 2D) [32]. The recombinant FBLN5-His was most likely not citrullinated because it did not react with AMC (Figure 2E). However, upon incubation with PAD2 *in vitro,* the FBLN5-His migrated slower probably due to changes in molecular weight and charge, and became strongly reactive to AMC, demonstrating PAD2-mediated citrullination. We then identified the sites of citrullination in FBLN5 by tandem mass spectrometry. For these studies, we followed the neutral loss of isocyanic acid (−CNOH, −43.0058 Da), which is unique to citrulline-containing ion fragments and is frequently observed during high-energy collision dissociation [33]. Using this method, protein coverage was 37% (red lines in Figure 2D) and we confirmed that R326, R351, and R408 were citrullinated (Figure 2D, 2F, and Supplemental Figure 2).

Attenuated elastogenesis in the absence of PAD activity

Both FBLN5 and LTBP4 are essential for elastogenesis. We therefore postulated that citrullination is critical for elastogenesis. We used an established pan-PAD inhibitor BB-Cl-amidine (BB) to inhibit citrullination [34]. Anti-elastin was then used to stain extracellular insoluble elastin as a readout for the formation of elastic fibers, a method widely used for visualizing elastic fibers [29, 35, 36]. In agreement with our hypothesis, BB dose-dependently inhibited *in vitro* elastogenesis of normal human dermal fibroblasts (NHDFs) (Figure 3A and 3B). The formation of elastic fibers was markedly inhibited with 0.75 μM

BB, a dose that had little impact on cell proliferation based on the number of nuclei present (Figure 3C). Only non-specific cellular staining was detected at 1 μM BB (Figure 3A). BB also dose-dependently reduced the level of intracellular PG-tagged FBLN5 (Figure 3D and 3E) but not the level of intracellular total FBLN5 (Figure 3D and 3F), suggesting that citrullination of FBLN5 occurs intracellularly. By contrast, BB had no impact on the protein level of intracellular elastin (Figure 3D) or the transcript level of other elastogenic proteins, such as LTBP4, FBLN4, LOX, and FBN1/2 (Figure 3G and Supplemental Figure 3A).

Attenuated elastogenesis and spontaneous emphysema in the absence of PAD2

Since BB may have off-target effects, we sought to further confirm the critical role of citrullination in elastogenesis by deriving lung fibroblasts from WT or PAD2KO neonates. The morphology of PAD2KO neonatal lung fibroblasts (NLFs) was indistinguishable from that of WT NLFs (Supplemental Figure 3B). More than 80% of the WT and PAD2KO NLFs were positive for podoplanin (Supplemental Figure 3C), a marker of fibroblasts, and negative for CD45, a marker for hematopoietic cells. We then subjected the NLFs to the *in vitro* elastogenesis assay. We found that PAD2KO NLFs formed elastic fibers much less robustly than WT NLFs (Figure 3H). The expression of several major elastogenic proteins (Figure 3I and Supplemental Figure 3D) and the cell recovery, based on the number of nuclei (Supplemental Figure 3E), were not affected by the absence of PAD2.

Poor quality of alveolar elastic fibers may result in high lung compliance, which is reversely correlated with elasticity, and render animals prone to emphysematous changes. Indeed, PAD2KO mice already exhibited higher lung compliance at 6-8 weeks of age (Figure 4A) despite grossly normal lung histology (Supplemental Figure 4A). To quantify histological changes, we converted images of H&E stain to skeletonized binary images and used the pixel count as a surrogate of airspace wall length, which should be reversely correlated with average alveolus size. There was indeed a subtle decrease in the pixel count of airspace wall length in 6-week-old PAD2KO mice (Supplemental Figure 4B and 4C). In addition, there were appreciable emphysematous changes in the lungs of 1-year-old PAD2KO mice (Figure 4B). The decrease in the pixel count of airspace wall per image (Figure 4C) and average count per mouse (Figure 4D) also became more obvious.

Restoration of elastogenesis in the absence of PAD activity with citrullinated FBLN5

FBLN5 is known to undergo protease-mediated cleavage events and cleaved FBLN5 is unable to participate in elastogenesis [35, 36]. While BB did not alter the intracellular level of full-length FBLN5 (Figure 3D), which has a molecular weight of 55 kDa, it dose-dependently reduced the level of full-length FBLN5 in supernatant (Figure 5A). Reciprocally, a 35 kDa protein that was also reactive to the anti-FBLN5 was induced by BB in the supernatant in a dose-dependent manner. This 35 kDa protein is very likely a fragment of FBLN5 that predominates at 1 μM of BB (Figure 5A and 5B); however, the combined level of the 55 kDa and 35 kDa proteins in the supernatant was not affected by BB (Figure 5C). The cleaved FBLN5 was also detected in the supernatant of PAD2KO NLFs (Figure 5A-5C), but there was still detectable full-length FBLN5 in the supernatant of PAD2KO NLFs, suggesting functional compensation by other PADs. As there was no FBLN5 cleavage detected inside BB-treated NHDFs (Figure 3D), its cleavage was most

likely carried out extracellularly by an arginine-directed protease. Indeed, the cleavage of FBLN5 was partially inhibited by the serine protease inhibitor Pefabloc SC but not by the cysteine protease inhibitor E-64 or matrix metallopeptidase inhibitor EDTA (Figure 5D). Unfortunately, all three inhibitors were cytotoxic to NHDFs even at low concentration (Supplemental Figure 5), precluding any analysis of their effect on elastogenesis.

To determine whether citrullinated FBLN5 was able to restore elastogenesis in the absence of PAD activity, we added the native and citrullinated FBLN5 shown in Figure 2E to BB-treated NHDFs. We found that the cit-FBLN5 partially restored elastogenesis (Figure 5E and 5F). There was visibly linear elastin staining albeit shorter and less dense than that was seen in untreated NHDFs. By contrast, exogenous native FBLN5-His yielded only sparse isolated staining nearly devoid of bright linear elastic fibers. This result indicates that the loss of elastic fiber staining is not due to the absence of extracellular elastin and shows that PAD2 promotes elastogenesis at least partially through a FBLN5-dependent mechanism.

Discussion

Our data have established a critical role of citrullination for elastogenesis (Figure 6). The citrullination of FBLN5 in lung is temporally regulated. Inhibition or deficiency of PAD2 facilitated the cleavage of FBLN5 and attenuated the ability of fibroblasts to form elastic fibers. This attenuated elastogenesis was partially rescued by citrullinated but not native FBLN5. More importantly, PAD2KO mice display abnormal lung physiology and histology resembling emphysema, a common outcome of attenuated elastogenesis or destruction of elastic fibers.

Citrullination can protect FBLN5 from proteolysis, thereby promoting elastogenesis. This FBLN5-dependent and cleavage-sensitive mechanism is consistent with a previous report showing that cleaved FBLN5 is unable to participate in elastogenesis probably due to attenuated interaction with LOXL1 [35]. One of the known cleavage sites in FBLN5 is between the arginine residue at position 77 (R77) and the glycine residue at position 78. The RG combination has been shown to be favored by PADs [37]. It is likely that citrullination of R77 neutralizes its positive charge and consequently abolishes this cleavage site of arginine-directed proteases. Unfortunately, R77 was not covered in our mass spectrometry. Additional mass spectrometry using different proteases will be needed to confirm the citrullination of R77. Thus, FBLN5 joins a small group of proteins, including CXCL8 and pro-Epidermal Growth Factor (EGF), whose cleavage has been shown to be prevented by citrullination. Citrullination of CXCL8 at R5 renders it resistant to digestion by thrombin or plasmin and dampens its chemotactic activity [38]; citrullination of pro-EGF by PAD4 at R1023 attenuates its cleavage by ADAM-like Decysin 1 and the release of soluble active EGF from platelets [39].

We and others have reported that FBLN5 can be cleaved by MMPs, porcine pancreatic elastase, Serine Protease 3, and a 25 kDa serine protease named V1 [32, 40, 41]. Interestingly, thrombin, an abundant arginine-directed protease, is ineffective in cleaving FBLN5 [40]. So far, the arginine-directed proteases responsible for cleaving FBLN5 in the absence of PAD2 activity are still unknown. Proteases typically are promiscuous in the

selection of target sites and often cleave secondary sites when their primary targets are not available. In addition, citrullination has also been shown to promote proteolysis of other proteins, such as myelin basic protein and filaggrin, probably by altering their folding and exposing target sites of non-arginine-directed proteases [42, 43]. Thus, citrullination may inhibit or enhance the proteolysis of FBLN5 depending on the position of peptidylcitrulline. Future studies on the proteolysis of FBLN5, and any other protein, will have to take into consideration of its status of citrullination. One may also ask why FBLN5 is not cleaved inside PAD2KO NLFs. There can be several explanations. FBLN5 and its proteases may be physically sequestered into different intracellular compartments; the proteases may be inactive intracellularly and become active only after they are secreted; and/or intracellular FBLN5 may be folded in a way that its proteases cannot access the cleavage sites. These scenarios will be subjects of future investigation.

There very likely also exist FBLN5-dependent and cleavage-insensitive mechanisms. FBLN5 interacts with the other elastogenic proteins mainly through the fibulin domain at its C-terminus, which contains three citrullinated sites, R326, R351, and R408. Citrullination of these three residues may be critical for the optimal interaction between FBLN5 and the other elastogenic proteins. Furthermore, the observation that cit-FBLN5 only partially restored elastogenesis of BB-treated NHDFs suggests that citrullination can also promote elastogenesis through FBLN5-independent mechanisms. PG-tagged LTBP4 was also enriched in young lungs in our proteomic analysis, suggesting that it is a PAD substrate. While FBLN4 was not present in the PG-tagged fraction in our proteomic analysis, FBLN4 can also recruit LOXL1 and is susceptible to cleavage [32]. Intriguingly, two of the three citrullinated residues of FBLN5, namely R351 and R408, are also present in FBLN4. It will be important to determine whether LTBP4 and FBLN4 are PAD substrates and whether their function is modulated by citrullination.

One very intriguing observation is that the activity of PAD2 in lung is temporally regulated in a substrate-specific manner. Both FBLN5 and Cyp2f2 are PAD2 substrates. PAD2-mediated citrullination of FBLN5 takes place mainly in young lungs, whereas citrullination of Cyp2f2 by PAD2 occurs preferentially in adult lungs. This reciprocal effect cannot be explained by a global change in PAD2 activity over age or by the mechanisms known to regulate PAD activity, such as calcium concentration, redox status [44], homodimerization [45], auto-citrullination [46], and interacting with PTPN22 [47], or the level of PAD2. One possible explanation is that environmental cues dictate PAD2's selection of its substrates. For instance, environmental signals encountered in early life favors the selection of FBLN5, whereas signals encountered in adult life favor Cyp2f2. This preferential selection can be achieved by regulating the physical interaction between PAD2 and its substrates within a single cell. Alternatively, this temporal regulation is a cell type-dependent phenomenon. For example, PAD2-mediated citrullination of FBLN5 and Cyp2f2 occur in different types of lung cells. Thus, PAD2 activity decreases along with age in cells expressing a high level of FBLN5, such as fibroblasts, but increases in non-fibroblasts expressing a high level of Cyp2f2. Either scenario would be intriguing and considered paradigm shifting. It will be also important to know whether the temporal citrullination of FBLN5 is also observed in other organs enriched or not enriched with elastic fibers.

Environmental factors may also explain why the temporal change in the level of cit-FBLN5 in human lungs is not as striking as that seen in mouse lungs. Microbiome and environmental pollutants have been shown to induce mucosal citrullination in human [48-50]. By contrast, the experimental mice are kept in an environment free of specific pathogens and pollutants. In addition, environmental factors may facilitate the degradation of elastic fibers in older human lungs, rendering the previously incorporated (and thus insoluble) cit-FBLN5 soluble and becoming detectable in the PG pulldown assay. If the latter scenario is true, then the released cit-FBLN5 is very likely in full-length because there was no detectable truncated FBLN5 in the human lungs from the older group.

FBLN5 can also interact with several integrins, including α5β1 and α4β1, through its RGD domain, thereby regulating cellular attachment, migration, and gene expression in an integrin-dependent manner [51-53]. In addition, several mis-sense mutations in FBLN5 have been linked to familial age-related macular degeneration and several forms of hereditary neuropathy [54, 55]. These functions of FBLN5 are very likely independent of its role in elastogenesis and could also be influenced by its citrullination through at least two mechanisms. First, citrullination of the RGD motif of TGF-β1-LAP has been confirmed by mass spectrometry and inhibits the binding of TGF-β1-LAP to αVβ6 integrin [56]. While citrullination of the RGD domain of FBLN5 was not identified in our mass spec analysis, it is still possible that it can be citrullinated by other PADs and that citrullination of the RGD domain of FBLN5 can interrupt its interaction with integrins. Second, the RGD domain is at the N-terminal end of FBLN5 and will be cleaved from native or hypocitrullinated FBLN5. Elucidating the role of citrullination in modulating the non-elastogenic functions of FBLN5 may lead to novel therapeutic approaches toward the FBLN5-assoicated diseases.

Experimental Procedures

Human lung samples

Human lung samples were procured from control lungs rejected for transplant per protocols approved by the Partners IRB (2011P002419) with informed consent.

Mice

The original source of PAD2KO mice was described previously [18, 57]. The mice have been backcrossed to DBA/1J mice for 12 generations. In all experiments involving PAD2KO DBA/1J mice or cells, wild type DBA/1J mice or cells were used as control. C57BL/6 mice were purchased from Jackson Laboratories (Bangor, ME). All mouse work was approved by BWH IACUC (2016N000479).

Human dermal fibroblasts and preparation of mouse lung fibroblasts

Normal adult human dermal fibroblasts (NHDFs-Ad, CC-2511) were purchased from Lonza (Basel, Switzerland) and were maintained in DMEM/F12 (Invitrogen) supplemented with 2 mM glutamine, penicillin/ streptomycin (100 units/mL and 100 μg/mL, respectively), and 10% fetal bovine serum at 37°C in 5% CO_2. Mouse lung fibroblasts were isolated according to a previously described method [58]. Briefly, neonatal mouse lungs were first perfused with sterile phosphate-buffered saline and removed *en bloc.* Collected lungs were

dissected, finely minced, and enzymatically digested for 90 min at 37°C in Dulbecco's modified Eagle's medium containing collagenase type I (0.5 mg/mL; Sigma-Aldrich) and collagenase type IA (0.5 mg/mL; Sigma-Aldrich), followed by pipetting to mechanically disperse lung tissue. The resulting cell suspension was then collected by centrifugation, resuspended in culture medium, and sequentially filtered through 100-, 70-, and 20- μm sterile filters. The filtrate from the 20-μm filter was plated on 60-mm cell culture dishes and cultured in Dulbecco's modified Eagle's medium with 10% fetal bovine serum, passaged and cryopreserved if needed for later use.

In vitro generation, staining, and quantification of elastic fibers

Fibroblasts treated with or without BB-Cl-amidine (Cayman Chemical, 1802637-39-3) were subconfluently plated on microscope cover glasses (12mm, Fisher Scientific) in 24-well plate and cultured in complete DMEM/F12 medium for 10 days. In some experiments, Pefabloc SC (Millipore Sigma, cat.# 11429868001), E-64 (Millipore Sigma, cat.#E3132), or EDTA (Millipore Sigma, cat.#E9884) was added along with BB-Cl-amidine. In *in vitro* FBLN5 rescue experiments, 6 μg/mL of native or citrullinated FBLN5 was added once the next day after cell plating. The cells were fixed with 100% methanol and blocked with 2% BSA. The primary antibodies used were anti-human elastin polyclonal (1/100; EPC Elastin Product Company, PR533), anti-human fibulin-5 polyclonal (1/100; Antibodies-online Inc., ABIN728473), or anti-mouse elastin polyclonal (1/100; EPC, PR387). The secondary antibodies used were Alexa Fluor 488 anti-rabbit or Alexa Fluor 594 anti-mouse IgG (1/200; Invitrogen). After staining with DAPI, stained cells were mounted with a Prolong Gold Antifade Kit (Invitrogen). Fluorescence images were sequentially collected through a Zeiss Axio Observer Z1 Inverted Microscope equipped with a Plan-Apochromat 63× objective, the Zeiss LSM 800 with Airyscan confocal package with Zeiss URGB (488 and 561 nm) laser lines, and Zen 2.3 blue edition confocal acquisition software. To objectively compare the amounts of elastic fibers, each image was separated by hue value to recreate images with exclusive DAPI, Alexa Fluor 488 staining, or Alexa Fluor 594 staining. Each exclusive image was subsequently converted to binary, using optimized parameters consistent for all processed images, where elastic fiber amounts may be quantified and normalized to number of cells detected per image.

Measurement of lung compliance

Lung compliance was measured with a Buxco® FinePoint Resistance and Compliance (Sharon, CT). Briefly, 6-week-old PAD2KO or WT mice were anesthetized with ketamine (100 mg/kg) in 100 μL of saline and tracheotomy was performed with an 18G stub needle cannula through a small incision in the skin overlying the trachea. When spontaneous breathing ceased, mice were placed on the ventilator and their lungs were inflated with room air at different rate. The air volume inflated into the lungs and the pressure in the lungs were monitored. Lung compliance was calculated by the following calculation: Lung Compliance (C) = Change in Lung Volume (V) / Change in Transpulmonary Pressure.

Real time PCR

RNA isolation, reverse transcription, and real time PCR were performed as previously described [59]. Transcript level thus detected was normalized against that of actin or HPRT. The sequences of the primers used are listed in Supplemental Table 4.

Western blotting

The following antibodies were used: anti-citrullinated histone H3 (ab5103) from Abcam (Cambridge, MA), anti-histone H3 (4620S) from Cell Signaling Technology (Danvers, MA), anti-Tubulin (T5168) from Sigma-Aldrich, F95 antibody (MABN328) and anti-AMC (MABS487) from EMD Serono (Rockland, MA), anti-FBLN5 (ABIN728473) from Antibodies-online (Limerick, PA), anti-human elastin (PR533) and anti-mouse elastin (PR385) from Elastin Product Company (Owensveille, OM). Densitometry readings of western blots were obtained with ImageJ software [60]. Loading controls were performed on the same gels after stripping unless indicated otherwise in the Figure Legends.

Generation and in vitro citrullination of FBLN5

Production of recombinant human FBLN5 followed a previously published procedure [32]. Briefly, stably transfected HEK293 cells were used to generate ~2.5 L conditioned serum-free culture medium containing secreted FBLN5. The medium was concentrated ~50-fold, dialyzed against 20 mM HEPES, 500 mM NaCl, pH 7.4 and purified using immobilized Ni^{2+}-affinity chromatography. Fractions containing FBLN5 with >90% purity were pooled, dialyzed against 150 mM NaCl, 2 mM $CaCl_2$, pH 7.4 and used for the experiments. Purified FBLN5 (0.162 mg/ml) was incubated with purified recombinant PAD2 (20 μM) for 4 hr at 37°C.

Biotinylated-PG pulldown

Cells or tissue extract were incubated with phenylglyoxal (PG)-biotin (0.1mM) in a buffer containing 50 mM HEPES and 20% trichloroacetic acid at 37°C for 30 min. After centrifugation, the pellet was resuspended in PBS containing 0.25% SDS, 0.14% BME, 0.4 mM HEPES (pH 7.6), 2 mM arginine, 2 mM NaCl. Biotin-PG labeled citrullinated proteins were captured with streptavidin–agarose beads (Thermo Fisher) over night at 4°C.

Mass spectrometry sample preparation

Organs were placed into a 2 mL. screw-cap plastic tube along with 1.4 mm ceramic beads and 1 mL. of cold lysis buffer (50 mM HEPES pH 7.6, 1 mM EDTA, 0.5 mM DTT, 0.5 mM PMSF). Tissue was lysed using a FastPrep24™ 5G homogenizer (MP) using factory-preset, tissue-specific protocols. Lysate was cleared via centrifugation at 17,000 x g on a tabletop centrifuge at 4°C for 20 min. Concentration of lysate was determined using a Bradford Assay.

Sample preparation was performed according to a published procedure [61]. Equal amounts of cell lysates from each experimental group (300 μg) were diluted in buffer (100 mM HEPES pH 7.6) to a final concentration of 1 μg/μL and incubated with 20% trichloroacetic acid (TCA) and 5 mM biotin-PG [62] for 30 min at 37 °C. Labeled proteins were

precipitated on ice for 30 min. Samples were pelleted via tabletop centrifugation (15,000 rpm, 15 min) at 4°C. The supernatants were discarded and the pellets were washed with cold acetone (300 μL). After drying for 5 min, the pellets were resuspended in 1.2% SDS in PBS by bath sonication and heating.

Samples were transferred to 15 mL screw cap tubes and diluted to 0.2% SDS in PBS. Samples were incubated with a streptavidin agarose slurry (Sigma Aldrich, 170 μL) overnight at 4°C and another 3 hr further at 25 °C. After discarding the flow through, the streptavidin beads were then washed with 0.2% SDS in PBS (5 mL.) for 10 min at 25 °C. The beads were then washed with PBS (5 mL. 3 times), and water (5 mL 3 times) in order to remove any unbound proteins. Beads were transferred to a screw cap microcentrifuge tube and heated in a buffer containing 500 μL 6 M urea in PBS and 10 mM DTT (65 °C, 20 min). Proteins bound to the beads were then alkylated with iodoacetamide (20 mM, 37°C for 30 min). The beads were then pelleted by centrifugation (1,400 x *g* for 3 min) and the supernatant was removed. The pellet was resuspended in 200 μL of a premixed solution composed of 2 M urea, 1 mM $CaCl_2$, and 2 μg Trypsin Gold (Promega) in PBS. These were agitated overnight at 37 °C. The supernatant was collected and the beads were washed with water (50 μL, 2X), each time collecting the eluent. The fractions were combined and acidified with formic acid (5% final concentration). These were then stored at −20°C until MS analysis.

Citrullinated FBLN5 was lyophilized and resolubilized in 2 M urea (30 μL) and 100 mM ammonium bicarbonate (70 μL) solution. Once dissolved, the samples were incubated with 1 M DTT (1.5 μL) for 15 min at 65 °C followed by incubation with 500 mM iodoacetamide (2.5 μL) for 30 min at room temperature. The samples were then treated with trypsin (1:40 dilution) overnight at 37 °C, dried using a SpeedVac and resolubilized in Buffer A (5% acetonitrile and 0.5% formic acid) and stored at −20 °C until MS analysis.

Mass spectrometry

Liquid chromatography-mass spectrometry/mass spectrometry (LC-MS/MS) analysis was performed on an LTQ-Orbitrap Discovery mass spectrometer (ThermoFisher) coupled to an Easy-nLC HPLC (ThermoFisher). Samples were pressure loaded onto a 250 μm fused-silica capillary hand packed with 4 cm Aqua C18 reverse phase resin (Phenomenex). Samples were separated on a hand packed 100 μm fused-silica capillary column with a 5 μm tip packed with 10 cm Aqua C18 reverse phase resin (Phenomenex). Peptides were eluted using a 10-hour gradient of 0-100% Buffer B in Buffer A (Buffer A: 95% water, 5% acetonitrile, 0.1% formic acid; Buffer B: 20% water, 80% acetonitrile, 0.1% formic acid). The flow rate through the column was set to ~400 nL/min and the spray voltage was set to 2.5 kV. One full MS scan (FTMS) was followed by 7 data-dependent MS2 scans (ITMS) of the n^{th} most abundant ions.

The tandem MS data of mouse lungs was searched using the SEQUEST algorithm using a concatenated target/decoy variant of the mouse UniProt database. A static modification of +57.02146 on cysteine was specified to account for alkylation by iodoacetamide. SEQUEST output files were filtered using DTASelect 2.0.

LC-MS/MS analysis

The peptides were reconstituted in a solution of 5% acetonitrile and 0.1% formic in water and injected into a nanoAcquity UPLC (Waters Corporation, Milford, MA) on an in-house packed pre-column (C18, 200A, 5μm, 2cm), followed by an in-house packed analytical column (C18, 100A, 3 μm, 25 cm). The aqueous mobile phase (A) was water + 0.1 % formic acid, and the organic mobile phase (B) was acetonitrile + 0.1 % formic acid. Peptides were trapped at a flow rate of 4 μL/min (for 4 min) and carried over to the analytical column at a flow rate of 300 nL/min using the following gradient: 5-35% B (for 60 min), 35-60% B (for 30 min) , 60% B (for 3 min) , 60-90% B (for 1 min), 90% B (for 15 min) , 90-5% B (for 1 min), 5%B (for 18 min). The peptide mixture was then injected into a Q Exactive hybrid quadrupole-Orbitrap (Thermo Fisher Scientific Inc., Waltham, MA) mass spectrometer using electrospray ionization voltage 1.45 kV in positive ionization mode. The data was acquired using the following parameters: MS1 data acquisition: MS resolution of 70,000 at m/z 200, AGC target of 1e6, maximum injection time of 30 ms, and m/z scan range of 300 to 1750. For MS2 data acquisition (in data-dependent acquisition (DDA) mode): MS resolution of 17,500 at m/z 200, AGC target of 1e5, maximum injection time of 110 ms, the isolation width of 1.6 Da, and HCD collision energy of 27 volts.

LC-MS/MS data processing

The raw data was processed and searched using Thermo Proteome Discoverer software (PD 2.1.1.21) (Thermo Fisher Scientific Inc.). To identify the citrullination sites in human FBLN5, the database search was performed against SwissProt human database by Mascot Server 2.6.2 (Matrix Science Ltd) in PD pipeline using the following search parameters: Tryptic digest with the maximum number of two missed cleavage sites per peptide, peptide precursor mass tolerance of 10 ppm, and fragment tolerance of 0.05 Da, dynamic modifications of peptide N-terminal glutamine to pyroglutamate, peptide N-terminal acetylation, methionine oxidation, citrullination on arginine, and deamidation on asparagine and glutamine, and static modification of carbamidomethyl on cysteine. The results were further processed using Scaffold 4.10.0 (Proteome Software Inc.). The neutral loss of −43 Da (−CHNO) on citrullinated arginine was imported to Scaffold using a custom UNIMOD file. The protein identification threshold was set to greater than 99% probability using Protein Prophet algorithms [63] applied in Scaffold. The minimum number of unique peptides per protein was set to 2, with 1% peptide Prophet FDR [64] applied in Scaffold. The mass spectrometry proteomics data have been deposited to the ProteomeXchange Consortium via the PRIDE [65] partner repository with the dataset identifier PXD026238.

Quantification of lung histology

Lung histology was analyzed with ImageJ. H&E images were converted to skeletonized binary images. The pixel counts of the skeletonized binary images were used as a surrogate of the length of airspace wall.

Statistical analysis

Statistical analysis was performed with unpaired Student’s t test in Figure 1G, 1H, 4A, 4C, 4D, and the right panel of 4F; paired t test in Figure 3B, 3C, 3H, and 4I; one-way ANOVA in

Figure 3E, the left panel of and 4F; and one-way ANOVA followed by multiple comparisons in Figure 2B and 2C.

Supplementary Material

Refer to Web version on PubMed Central for supplementary material.

Acknowledgements:

We thank Dr. Roshanak Aslebagh and Dr. Scott Shaffer of UMass Proteomic Core for carrying out mass spectrometry analysis.

Funding:

This work was supported by grants AR070171 (to ICH), AR070253 (to BS), AI095219 (to TL), AR074558 (to KT), and GM118112 (to PRT) from the National Institutes of Health, and RGPIN-2016-06278 (to DPR) from the Natural Sciences and Engineering Research Council of Canada.

References

[1]. Nakamura T, Roles of short fibulins, a family of matricellular proteins, in lung matrix assembly and disease, Matrix biology : journal of the International Society for Matrix Biology 73 (2018) 21–33. [PubMed: 29412171]

[2]. Kozel BA, Mecham RP, Elastic fiber ultrastructure and assembly, Matrix biology : journal of the International Society for Matrix Biology 84 (2019) 31–40. [PubMed: 31669522]

[3]. Berk DR, Bentley DD, Bayliss SJ, Lind A, Urban Z, Cutis laxa: a review, J Am Acad Dermatol 66(5) (2012) 842 e1–17. [PubMed: 22387031]

[4]. Shapiro SD, Endicott SK, Province MA, Pierce JA, Campbell EJ, Marked longevity of human lung parenchymal elastic fibers deduced from prevalence of D-aspartate and nuclear weapons-related radiocarbon, The Journal of clinical investigation 87(5) (1991) 1828–34. [PubMed: 2022748]

[5]. Ding H, Gray SD, Senescent expression of genes coding tropoelastin, elastase, lysyl oxidase, and tissue inhibitors of metalloproteinases in rat vocal folds: comparison with skin and lungs, J Speech Lang Hear Res 44(2) (2001) 317–26. [PubMed: 11324654]

[6]. Deslee G, Woods JC, Moore CM, Liu L, Conradi SH, Milne M, Gierada DS, Pierce J, Patterson A, Lewit RA, Battaile JT, Holtzman MJ, Hogg JC, Pierce RA, Elastin expression in very severe human COPD, Eur Respir J 34(2) (2009) 324–331. [PubMed: 19357152]

[7]. Zhang J, Wu L, Qu JM, Bai CX, Merrilees MJ, Black PN, Pro-inflammatory phenotype of COPD fibroblasts not compatible with repair in COPD lung, J Cell Mol Med 16(7) (2012) 1522–32. [PubMed: 22117690]

[8]. Bonifazi M, Montero MA, Renzoni EA, Idiopathic Pleuroparenchymal Fibroelastosis, Curr Pulmonol Rep 6(1) (2017) 9–15. [PubMed: 28344924]

[9]. Witalison EE, Thompson PR, Hofseth LJ, Protein Arginine Deiminases and Associated Citrullination: Physiological Functions and Diseases Associated with Dysregulation, Current drug targets 16(7) (2015) 700–10. [PubMed: 25642720]

[10]. Zhang X, Liu X, Zhang M, Li T, Muth A, Thompson PR, Coonrod SA, Zhang X, Peptidylarginine deiminase 1-catalyzed histone citrullination is essential for early embryo development, Scientific reports 6 (2016) 38727. [PubMed: 27929094]

[11]. Clancy KW, Russell AM, Subramanian V, Nguyen H, Qian Y, Campbell RM, Thompson PR, Citrullination/Methylation Crosstalk on Histone H3 Regulates ER-Target Gene Transcription, ACS chemical biology 12(6) (2017) 1691–1702. [PubMed: 28485572]

[12]. Christophorou MA, Castelo-Branco G, Halley-Stott RP, Oliveira CS, Loos R, Radzisheuskaya A, Mowen KA, Bertone P, Silva JC, Zernicka-Goetz M, Nielsen ML, Gurdon JB, Kouzarides T, Citrullination regulates pluripotency and histone H1 binding to chromatin, Nature 507(7490) (2014) 104–8. [PubMed: 24463520]

[13]. Ghari F, Quirke AM, Munro S, Kawalkowska J, Picaud S, McGouran J, Subramanian V, Muth A, Williams R, Kessler B, Thompson PR, Fillipakopoulos P, Knapp S, Venables PJ, La Thangue NB, Citrullination-acetylation interplay guides E2F-1 activity during the inflammatory response, Science advances 2(2) (2016) e1501257. [PubMed: 26989780]

[14]. Sharma P, Azebi S, England P, Christensen T, Moller-Larsen A, Petersen T, Batsche E, Muchardt C, Citrullination of histone H3 interferes with HP1-mediated transcriptional repression, PLoS genetics 8(9) (2012) e1002934. [PubMed: 23028349]

[15]. Sun B, Dwivedi N, Bechtel TJ, Paulsen JL, Muth A, Bawadekar M, Li G, Thompson PR, Shelef MA, Schiffer CA, Weerapana E, Ho IC, Citrullination of NF-kappaB p65 promotes its nuclear localization and TLR-induced expression of IL-1beta and TNFalpha, Sci Immunol 2(12) (2017).

[16]. Sun B, Chang HH, Salinger A, Tomita B, Bawadekar M, Holmes CL, Shelef MA, Weerapana E, Thompson PR, Ho IC, Reciprocal regulation of Th2 and Th17 cells by PAD2-mediated citrullination, JCI insight 4(22) (2019).

[17]. Leshner M, Wang S, Lewis C, Zheng H, Chen XA, Santy L, Wang Y, PAD4 mediated histone hypercitrullination induces heterochromatin decondensation and chromatin unfolding to form neutrophil extracellular trap-like structures, Frontiers in immunology 3 (2012) 307. [PubMed: 23060885]

[18]. Li P, Li M, Lindberg MR, Kennett MJ, Xiong N, Wang Y, PAD4 is essential for antibacterial innate immunity mediated by neutrophil extracellular traps, The Journal of experimental medicine 207(9) (2010) 1853–62. [PubMed: 20733033]

[19]. FB UB, Cau L, Tafazzoli A, Mechin MC, Wolf S, Romano MT, Valentin F, Wiegmann H, Huchenq A, Kandil R, Garcia Bartels N, Kilic A, George S, Ralser DJ, Bergner S, Ferguson DJ, Oprisoreanu AM, Wehner M, Thiele H, Altmuller J, Nurnberg P, Swan D, Houniet D, Buchner A, Weibel L, Wagner N, Grimalt R, Bygum A, Serre G, Blume-Peytavi U, Sprecher E, Schoch S, Oji V, Hamm H, Farrant P, Simon M, Betz RC, Mutations in Three Genes Encoding Proteins Involved in Hair Shaft Formation Cause Uncombable Hair Syndrome, American journal of human genetics 99(6) (2016) 1292–1304. [PubMed: 27866708]

[20]. Malki L, Sarig O, Romano MT, Mechin MC, Peled A, Pavlovsky M, Warshauer E, Samuelov L, Uwakwe L, Briskin V, Mohamad J, Gat A, Isakov O, Rabinowitz T, Shomron N, Adir N, Simon M, McMichael A, Dlova NC, Betz RC, Sprecher E, Variant PADI3 in Central Centrifugal Cicatricial Alopecia, The New England journal of medicine 380(9) (2019) 833–841. [PubMed: 30763140]

[21]. Boon L, Ugarte-Berzal E, Martens E, Fiten P, Vandooren J, Janssens R, Blanter M, Yu K, Boon M, Struyf S, Proost P, Opdenakker G, Citrullination as a novel posttranslational modification of matrix metalloproteinases, Matrix biology : journal of the International Society for Matrix Biology 95 (2021) 68–83. [PubMed: 33157227]

[22]. Stefanelli VL, Choudhury S, Hu P, Liu Y, Schwenzer A, Yeh CR, Chambers DM, Pesson K, Li W, Segura T, Midwood KS, Torres M, Barker TH, Citrullination of fibronectin alters integrin clustering and focal adhesion stability promoting stromal cell invasion, Matrix biology : journal of the International Society for Matrix Biology 82 (2019) 86–104. [PubMed: 31004743]

[23]. Nicholas AP, Whitaker JN, Preparation of a monoclonal antibody to citrullinated epitopes: its characterization and some applications to immunohistochemistry in human brain, Glia 37(4) (2002) 328–36. [PubMed: 11870872]

[24]. Senshu T, Sato T, Inoue T, Akiyama K, Asaga H, Detection of citrulline residues in deiminated proteins on polyvinylidene difluoride membrane, Analytical biochemistry 203(1) (1992) 94–100. [PubMed: 1524220]

[25]. Chou KC, Shen HB, A new method for predicting the subcellular localization of eukaryotic proteins with both single and multiple sites: Euk-mPLoc 2.0, PloS one 5(4) (2010) e9931. [PubMed: 20368981]

[26]. Szklarczyk D, Gable AL, Lyon D, Junge A, Wyder S, Huerta-Cepas J, Simonovic M, Doncheva NT, Morris JH, Bork P, Jensen LJ, Mering CV, STRING v11: protein-protein association networks with increased coverage, supporting functional discovery in genome-wide experimental datasets, Nucleic acids research 47(D1) (2019) D607–D613. [PubMed: 30476243]

[27]. Nakamura T, Lozano PR, Ikeda Y, Iwanaga Y, Hinek A, Minamisawa S, Cheng CF, Kobuke K, Dalton N, Takada Y, Tashiro K, Ross J Jr., Honjo T, Chien KR, Fibulin-5/DANCE is essential for elastogenesis in vivo, Nature 415(6868) (2002) 171–5. [PubMed: 11805835]

[28]. Yanagisawa H, Davis EC, Starcher BC, Ouchi T, Yanagisawa M, Richardson JA, Olson EN, Fibulin-5 is an elastin-binding protein essential for elastic fibre development in vivo, Nature 415(6868) (2002) 168–71. [PubMed: 11805834]

[29]. Noda K, Dabovic B, Takagi K, Inoue T, Horiguchi M, Hirai M, Fujikawa Y, Akama TO, Kusumoto K, Zilberberg L, Sakai LY, Koli K, Naitoh M, von Melchner H, Suzuki S, Rifkin DB, Nakamura T, Latent TGF-beta binding protein 4 promotes elastic fiber assembly by interacting with fibulin-5, Proceedings of the National Academy of Sciences of the United States of America 110(8) (2013) 2852–7. [PubMed: 23382201]

[30]. Kumra H, Nelea V, Hakami H, Pagliuzza A, Djokic J, Xu J, Yanagisawa H, Reinhardt DP, Fibulin-4 exerts a dual role in LTBP-4L-mediated matrix assembly and function, Proceedings of the National Academy of Sciences of the United States of America 116(41) (2019) 20428–20437. [PubMed: 31548410]

[31]. Tilvawala R, Nguyen SH, Maurais AJ, Nemmara VV, Nagar M, Salinger AJ, Nagpal S, Weerapana E, Thompson PR, The Rheumatoid Arthritis-Associated Citrullinome, Cell chemical biology (2018).

[32]. Djokic J, Fagotto-Kaufmann C, Bartels R, Nelea V, Reinhardt DP, Fibulin−3, −4, and −5 are highly susceptible to proteolysis, interact with cells and heparin, and form multimers, The Journal of biological chemistry 288(31) (2013) 22821–35. [PubMed: 23782690]

[33]. Lee CY, Wang D, Wilhelm M, Zolg DP, Schmidt T, Schnatbaum K, Reimer U, Ponten F, Uhlen M, Hahne H, Kuster B, Mining the human tissue proteome for protein citrullination, Molecular & cellular proteomics : MCP (2018).

[34]. Knight JS, Subramanian V, O'Dell AA, Yalavarthi S, Zhao W, Smith CK, Hodgin JB, Thompson PR, Kaplan MJ, Peptidylarginine deiminase inhibition disrupts NET formation and protects against kidney, skin and vascular disease in lupus-prone MRL/lpr mice, Annals of the rheumatic diseases (2014).

[35]. Hirai M, Ohbayashi T, Horiguchi M, Okawa K, Hagiwara A, Chien KR, Kita T, Nakamura T, Fibulin-5/DANCE has an elastogenic organizer activity that is abrogated by proteolytic cleavage in vivo, The Journal of cell biology 176(7) (2007) 1061–71. [PubMed: 17371835]

[36]. Zheng Q, Davis EC, Richardson JA, Starcher BC, Li T, Gerard RD, Yanagisawa H, Molecular analysis of fibulin-5 function during de novo synthesis of elastic fibers, Molecular and cellular biology 27(3) (2007) 1083–95. [PubMed: 17130242]

[37]. Assohou-Luty C, Raijmakers R, Benckhuijsen WE, Stammen-Vogelzangs J, de Ru A, van Veelen PA, Franken KL, Drijfhout JW, Pruijn GJ, The human peptidylarginine deiminases type 2 and type 4 have distinct substrate specificities, Biochimica et biophysica acta 1844(4) (2014) 829–36. [PubMed: 24594197]

[38]. Proost P, Loos T, Mortier A, Schutyser E, Gouwy M, Noppen S, Dillen C, Ronsse I, Conings R, Struyf S, Opdenakker G, Maudgal PC, Van Damme J, Citrullination of CXCL8 by peptidylarginine deiminase alters receptor usage, prevents proteolysis, and dampens tissue inflammation, The Journal of experimental medicine 205(9) (2008) 2085–97. [PubMed: 18710930]

[39]. Chen R, Jin G, McIntyre TM, The soluble protease ADAMDEC1 released from activated platelets hydrolyzes platelet membrane pro-epidermal growth factor (EGF) to active high-molecular-weight EGF, The Journal of biological chemistry 292(24) (2017) 10112–10122. [PubMed: 28455445]

[40]. Manders DB, Kishore HA, Gazdar AF, Keller PW, Tsunezumi J, Yanagisawa H, Lea J, Word RA, Dysregulation of fibulin-5 and matrix metalloproteases in epithelial ovarian cancer, Oncotarget 9(18) (2018) 14251–14267. [PubMed: 29581841]

[41]. Budatha M, Silva S, Montoya TI, Suzuki A, Shah-Simpson S, Wieslander CK, Yanagisawa M, Word RA, Yanagisawa H, Dysregulation of protease and protease inhibitors in a mouse model of human pelvic organ prolapse, PloS one 8(2) (2013) e56376. [PubMed: 23437119]

[42]. Pritzker LB, Joshi S, Gowan JJ, Harauz G, Moscarello MA, Deimination of myelin basic protein. 1. Effect of deimination of arginyl residues of myelin basic protein on its structure

and susceptibility to digestion by cathepsin D, Biochemistry 39(18) (2000) 5374–81. [PubMed: 10820008]

[43]. Kamata Y, Taniguchi A, Yamamoto M, Nomura J, Ishihara K, Takahara H, Hibino T, Takeda A, Neutral cysteine protease bleomycin hydrolase is essential for the breakdown of deiminated filaggrin into amino acids, The Journal of biological chemistry 284(19) (2009) 12829–36. [PubMed: 19286660]

[44]. Nagar M, Tilvawala R, Thompson PR, Thioredoxin Modulates Protein Arginine Deiminase 4 (PAD4)-Catalyzed Citrullination, Frontiers in immunology 10 (2019) 244. [PubMed: 30853960]

[45]. Arita K, Hashimoto H, Shimizu T, Nakashima K, Yamada M, Sato M, Structural basis for Ca(2+)-induced activation of human PAD4, Nature structural & molecular biology 11(8) (2004) 777–83.

[46]. Andrade F, Darrah E, Gucek M, Cole RN, Rosen A, Zhu X, Autocitrullination of human peptidyl arginine deiminase type 4 regulates protein citrullination during cell activation, Arthritis and rheumatism 62(6) (2010) 1630–40. [PubMed: 20201080]

[47]. Chang HH, Dwivedi N, Nicholas AP, Ho IC, The W620 Polymorphism in PTPN22 Disrupts Its Interaction With Peptidylarginine Deiminase Type 4 and Enhances Citrullination and NETosis, Arthritis Rheumatol 67(9) (2015) 2323–34. [PubMed: 26019128]

[48]. Jenning M, Marklein B, Ytterberg J, Zubarev RA, Joshua V, van Schaardenburg D, van de Stadt L, Catrina AI, Nonhoff U, Haupl T, Konthur Z, Burmester GR, Skriner K, Bacterial citrullinated epitopes generated by Porphyromonas gingivalis infection-a missing link for ACPA production, Annals of the rheumatic diseases 79(9) (2020) 1194–1202. [PubMed: 32532752]

[49]. Makrygiannakis D, Hermansson M, Ulfgren AK, Nicholas AP, Zendman AJ, Eklund A, Grunewald J, Skold CM, Klareskog L, Catrina AI, Smoking increases peptidylarginine deiminase 2 enzyme expression in human lungs and increases citrullination in BAL cells, Annals of the rheumatic diseases 67(10) (2008) 1488–92. [PubMed: 18413445]

[50]. Li FJ, Surolia R, Li H, Wang Z, Liu G, Kulkarni T, Massicano AVF, Mobley JA, Mondal S, de Andrade JA, Coonrod SA, Thompson PR, Wille K, Lapi SE, Athar M, Thannickal VJ, Carter AB, Antony VB, Citrullinated vimentin mediates development and progression of lung fibrosis, Science translational medicine 13(585) (2021).

[51]. Lomas AC, Mellody KT, Freeman LJ, Bax DV, Shuttleworth CA, Kielty CM, Fibulin-5 binds human smooth-muscle cells through alpha5beta1 and alpha4beta1 integrins, but does not support receptor activation, The Biochemical journal 405(3) (2007) 417–28. [PubMed: 17472576]

[52]. Yue W, Sun Q, Landreneau R, Wu C, Siegfried JM, Yu J, Zhang L, Fibulin-5 suppresses lung cancer invasion by inhibiting matrix metalloproteinase-7 expression, Cancer research 69(15) (2009) 6339–46. [PubMed: 19584278]

[53]. Schluterman MK, Chapman SL, Korpanty G, Ozumi K, Fukai T, Yanagisawa H, Brekken RA, Loss of fibulin-5 binding to beta1 integrins inhibits tumor growth by increasing the level of ROS, Disease models & mechanisms 3(5-6) (2010) 333–42. [PubMed: 20197418]

[54]. Auer-Grumbach M, Weger M, Fink-Puches R, Papic L, Frohlich E, Auer-Grumbach P, El Shabrawi-Caelen L, Schabhuttl M, Windpassinger C, Senderek J, Budka H, Trajanoski S, Janecke AR, Haas A, Metze D, Pieber TR, Guelly C, Fibulin-5 mutations link inherited neuropathies, age-related macular degeneration and hyperelastic skin, Brain 134(Pt 6) (2011) 1839–52. [PubMed: 21576112]

[55]. Stone EM, Braun TA, Russell SR, Kuehn MH, Lotery AJ, Moore PA, Eastman CG, Casavant TL, Sheffield VC, Missense variations in the fibulin 5 gene and age-related macular degeneration, The New England journal of medicine 351(4) (2004) 346–53. [PubMed: 15269314]

[56]. Sipila KH, Ranga V, Rappu P, Torittu A, Pirila L, Kapyla J, Johnson MS, Larjava H, Heino J, Extracellular citrullination inhibits the function of matrix associated TGF-beta, Matrix biology : journal of the International Society for Matrix Biology 55 (2016) 77–89. [PubMed: 26923761]

[57]. Raijmakers R, Vogelzangs J, Raats J, Panzenbeck M, Corby M, Jiang H, Thibodeau M, Haynes N, van Venrooij WJ, Pruijn GJ, Werneburg B, Experimental autoimmune encephalomyelitis induction in peptidylarginine deiminase 2 knockout mice, The Journal of comparative neurology 498(2) (2006) 217–26. [PubMed: 16856138]

[58]. Benjamin JT, van der Meer R, Im AM, Plosa EJ, Zaynagetdinov R, Burman A, Havrilla ME, Gleaves LA, Polosukhin VV, Deutsch GH, Yanagisawa H, Davidson JM, Prince LS, Young LR, Blackwell TS, Epithelial-Derived Inflammation Disrupts Elastin Assembly and Alters Saccular Stage Lung Development, The American journal of pathology 186(7) (2016) 1786–1800. [PubMed: 27181406]

[59]. Chang HH, Miaw SC, Tseng W, Sun YW, Liu CC, Tsao HW, Ho IC, PTPN22 modulates macrophage polarization and susceptibility to dextran sulfate sodium-induced colitis, J Immunol 191(5) (2013) 2134–43. [PubMed: 23913970]

[60]. Schneider CA, Rasband WS, Eliceiri KW, NIH Image to ImageJ: 25 years of image analysis, Nature methods 9(7) (2012) 671–5. [PubMed: 22930834]

[61]. Tilvawala R, Nguyen SH, Maurais AJ, Nemmara VV, Nagar M, Salinger AJ, Nagpal S, Weerapana E, Thompson PR, The Rheumatoid Arthritis-Associated Citrullinome, Cell chemical biology 25(6) (2018) 691–704 e6. [PubMed: 29628436]

[62]. Lewallen DM, Bicker KL, Subramanian V, Clancy KW, Slade DJ, Martell J, Dreyton CJ, Sokolove J, Weerapana E, Thompson PR, Chemical Proteomic Platform To Identify Citrullinated Proteins, ACS Chemical Biology 10(11) (2015) 2520–2528. [PubMed: 26360112]

[63]. Nesvizhskii AI, Keller A, Kolker E, Aebersold R, A statistical model for identifying proteins by tandem mass spectrometry, Anal Chem 75(17) (2003) 4646–58. [PubMed: 14632076]

[64]. Keller A, Nesvizhskii AI, Kolker E, Aebersold R, Empirical statistical model to estimate the accuracy of peptide identifications made by MS/MS and database search, Anal Chem 74(20) (2002) 5383–92. [PubMed: 12403597]

[65]. Perez-Riverol Y, Csordas A, Bai J, Bernal-Llinares M, Hewapathirana S, Kundu DJ, Inuganti A, Griss J, Mayer G, Eisenacher M, Perez E, Uszkoreit J, Pfeuffer J, Sachsenberg T, Yilmaz S, Tiwary S, Cox J, Audain E, Walzer M, Jarnuczak AF, Ternent T, Brazma A, Vizcaino JA, The PRIDE database and related tools and resources in 2019: improving support for quantification data, Nucleic acids research 47(D1) (2019) D442–D450. [PubMed: 30395289]

Highlights

- FBLN5 is a substrate of PAD2 and its citrullination in lungs undergoes a temporal change correlating with in vivo elastogenesis.
- Citrullination of FBLN5 protects it from cleavage by serine proteases and is essential for its elastogenic function.
- Pharmacological inhibition of PAD activity or genetic deficiency of PAD2 attenuates in vitro elastogenesis of normal human dermal fibroblasts or mouse neonatal lung fibroblasts, respectively.
- Exogeneous citrullinated FBLN5, but not native FBLN5, partially rescues in vitro elastogenesis in the absence of PAD activity.
- PAD2-deficient mice display heightened lung compliance at an early age and develop age-dependent emphysema.

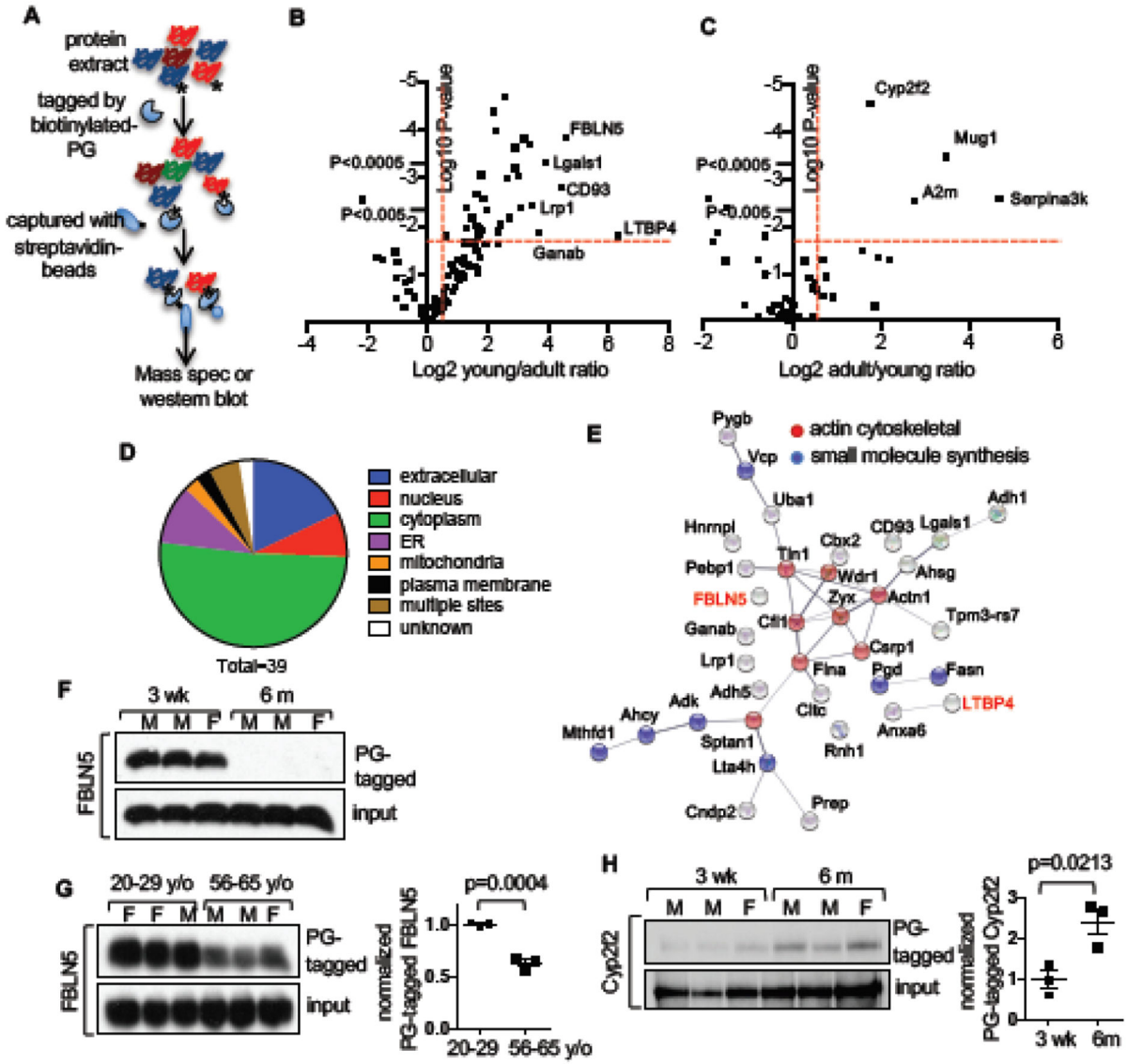

Figure 1. Identification of PG-tagged lung proteins enriched in different age groups.

A. Schematic diagram of the method for identification of PG-tagged proteins. * represents peptidylcitrulline. **B-E**. Lung extract from WT young (3-week-old) and adult (6-month-old) C57BL/6 mice was subjected to the PG pulldown and the PG-tagged proteins were identified by mass spectrometry. The PG-tagged proteins enriched in young and adult lungs are shown in the volcano plot in **B** and **C**, respectively. The subcellular distribution of the PG-tagged proteins thus identified is shown in the pie chart in **D**. The proteins were analyzed with STRING. Their interaction network is shown in **E**. **F-H.** The temporal enrichment of PG-tagged FBLN5 (**F** & **G**) and Cyp2f2 (**H**) in mouse (**F** & **H**) and human (**G**) lungs was confirmed by western blotting. The normalized density of PG-tagged FBLN5 and Cyp2f2 is shown in the dot plot of **G** and **H**, respectively. M and F stand for male and female, respectively.

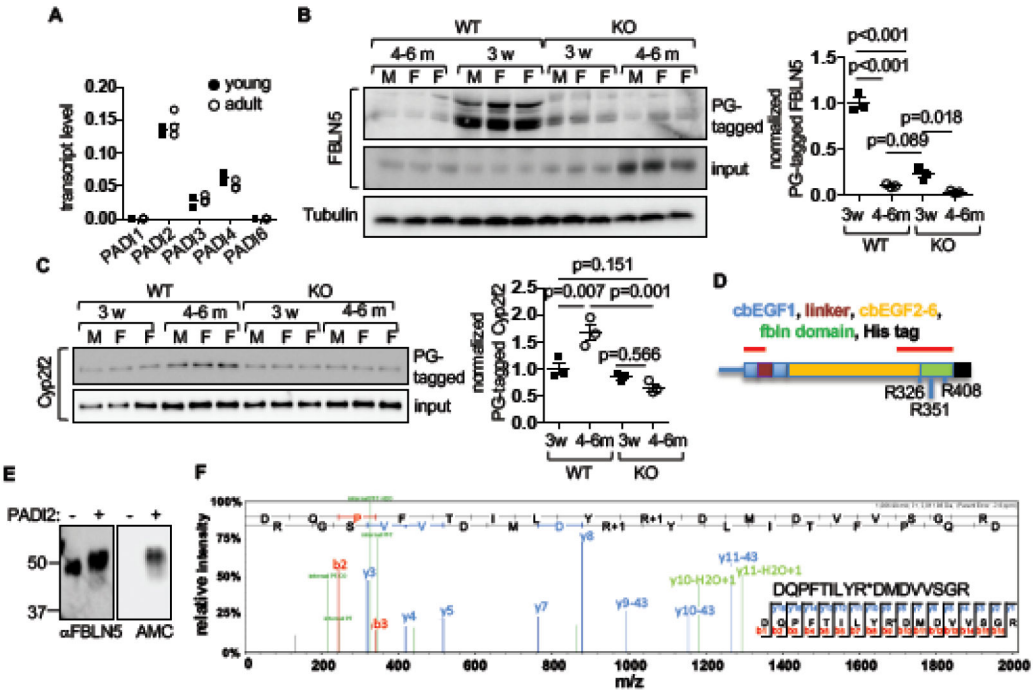

Figure 2. Temporal citrullination of FBLN5 by PAD2.

A. The transcript level of various PADs in the lung of 3-week-old (young, N=3) and 6-month-old (adult, N=3) mice was quantified with qPCR. **B & C**. Lung extract of WT and PAD2KO mice of indicated ages was subjected to PG-pulldown followed by western blotting or directly to western blotting with anti-FBLN5 (**B**), anti-tubulin (**B**), or anti-Cyp2f2 (**C**). The density of protein bands was quantified with densitometry and the density of PG-tagged FBLN5 and Cyp2f2 was normalized against that of input FBLN5 and Cyp2f2. The normalized density of PG-tagged FBLN5 and Cyp2f2 is shown in the dot plot of **B** and **C**, respectively. M and F stand for male and female, respectively. **D-F**. Recombinant human FBLN5 was produced by HEK293 cells and purified to homogeneity. A schematic diagram of FBLN5 is shown in **D**. The structural domains are designated by colors. cbEGF stands for calcium binding EGF domain and fbln stands for the unique C-terminal fibulin domain. FBLN5 was left un-treated or incubated with PAD2, then analyzed by western blotting using anti-FBLN5 or AMC (**E**). The citrullinated FBLN5 was then subjected to mass spectrometry. The sequences covered by mass spectrometry are indicated with red lines and the position of three citrullinated residues (R326, R351, and R408) identified by mass spectrometry are indicated in **D**. The MS2 tracing of R351 is shown in **F**.

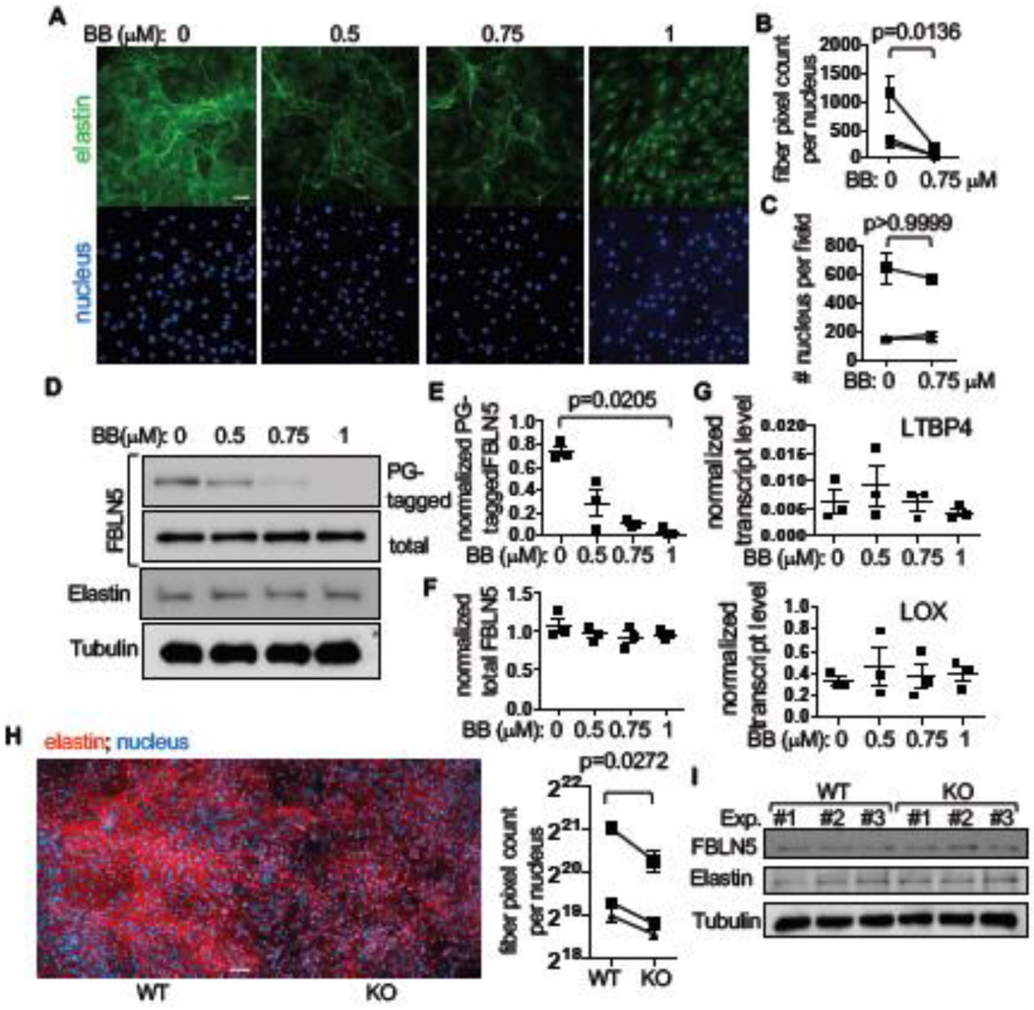

Figure 3. Regulation of elastogenesis by PAD2-mediated citrullination.

A-G. NHDFs were cultivated in the presence of BB-Cl-amidine (BB) at indicated concentration and subjected to staining with DAPI and anti-elastin. Representative images from three experiments are shown in **A**. The pixel count of the elastin stain in each field was normalized against the number of nucleus. At least 6 fields per slide were analyzed. The mean and SEM of the normalized elastin pixel count (0 μM vs 0.75 μM) are shown in **B**. The mean and SEM of nucleus numbers are shown in **C**. Data from the same experiments are connected with lines in **B** and **C**. Whole cell extract from the BB-treated NHDFs was analyzed directly by western blotting using the indicated antibodies or subjected to PG pulldown first before western blotting with anti-FBLN5. Representative western blots are shown in **D**. Normalized density of PG-tagged FBLN5 and total FBLN5 is shown in **E** and **F**, respectively. The transcript levels of LTBP4 and LOX are shown in **G**. **H** & **I.** WT and PAD2KO NLFs were subjected to staining with DAPI and anti-elastin. Representative images from three experiments are shown in **H**. The mean and SEM of the normalized elastin pixel counts (at least 5 fields per slide) are shown in the dot plot. Data points from the same experiments are connected with lines. The intracellular levels of indicated proteins

were quantified by western blotting (**I**). The white horizontal bars in the right lower corer of each image indicate 50 μm.

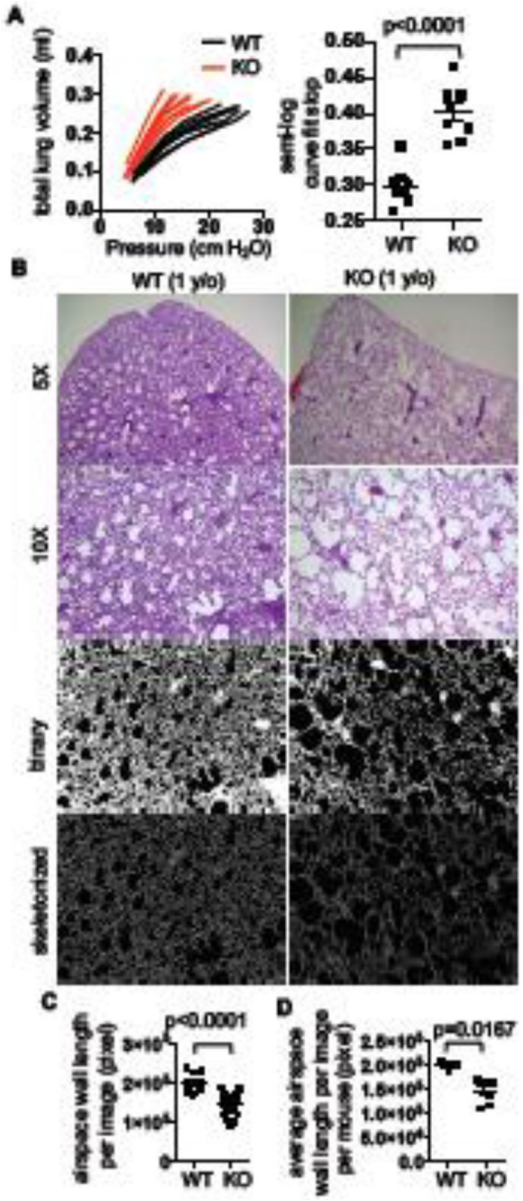

Figure 4. Spontaneous emphysema in the absence of PAD2.

A. WT and PAD2KO mice (6-8-week-old) were subjected to measurement of lung compliance. The pressure/volume curves from two experiments (PAD2KO, N=9, 5 male, 4 female; WT, N=8, 5 male, 3 female) are shown. The curve fit slops are shown in the dot plot. **B-D**. Lungs harvested from 1-year-old WT (N=3, 1 male and 2 female) and PAD2KO (N=7, 2 male and 5 female) mice were subjected to H&E staining. Representative H&E and their skeletonized binary images are shown in **B**. The white bar in the right lower corner of each image indicates 50 μm. The pixel counts of the skeletonized binary images (4 images per mouse) were quantified with ImageJ. The pixel counts from all images are shown in **C** and the average pixel counts per image per mouse are shown in **D** (2 pixels = 1 μm).

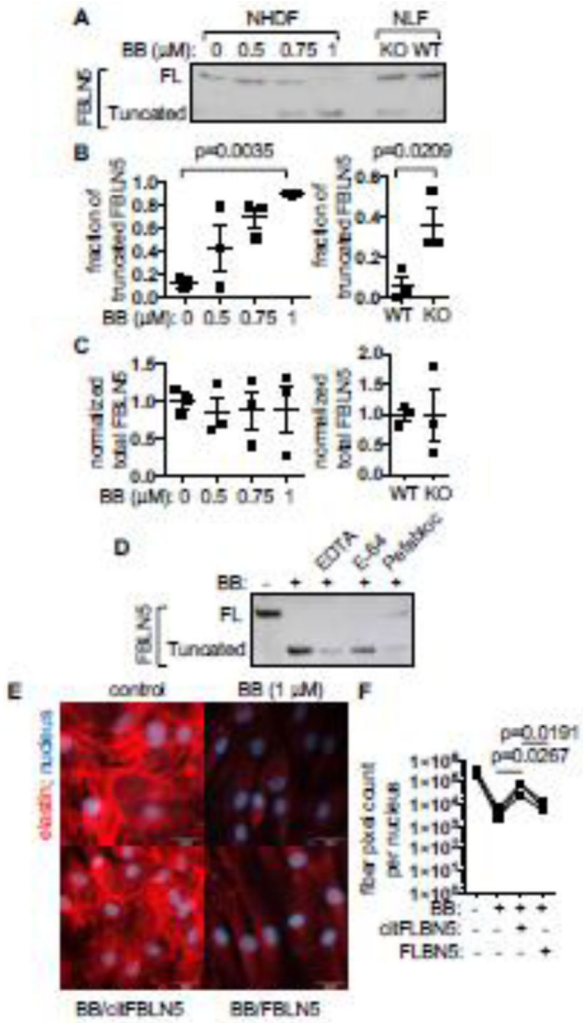

Figure 5. Restoration of elastogenesis in the absence of PAD activity with citrullinated FBLN5.

A-C. The supernatant (150 μL/lane) of NHDFs untreated or treated with indicated concentration of BB, along with the supernatant of WT and PAD2KO NLFs were subjected to western blotting using anti-FBLN5. Representative western blots from three experiments are shown in **A.** The full-length (FL) and truncated FBLN5 are marked. The fraction of cleaved FBLN5 and total FBLN5 (FL + cleaved FBLN5) (mean and SEM) are shown in **B** and **C**, respectively. **D.** NHDFs were treated with BB (1 μM) along with Pefabloc SC (50 μg/mL), E-64 (5 μM), or EDTA (50 μM). The presence of FBLN5 in supernatant was examined with western blotting. **E & F**. Native and citrullinated FBLN5 were added to BB-treated NHDFs. The formation of elastic fibers was examined by elastin staining. Representative images from three experiments are shown in **E**. The mean of normalized pixel counts of elastin from 5 images per sample are shown in **F**. Data points from the same experiments are connected with lines. The white bar in the right lower corner of each image in **E** indicates 20 μm.

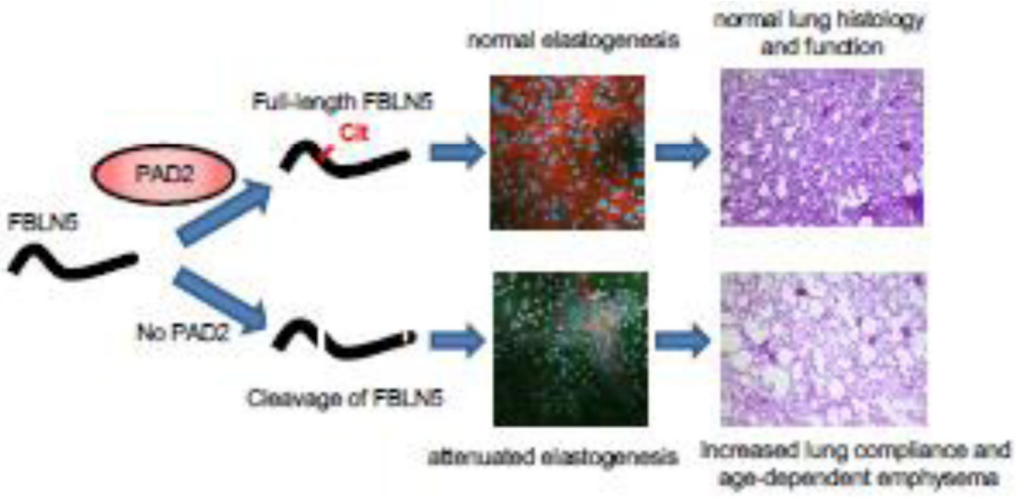

Figure 6.

A working model showing that PAD2 promotes elastogenesis by protecting FBLN5 from proteolysis.